

**Spectroscopy of the neutron-rich actinide nucleus  $^{240}\text{U}$  following multinucleon-transfer reactions**

B. Birkenbach,<sup>1,\*</sup> A. Vogt,<sup>1</sup> K. Geibel,<sup>1</sup> F. Recchia,<sup>2,3</sup> P. Reiter,<sup>1</sup> J. J. Valiente-Dobón,<sup>4</sup> D. Bazzacco,<sup>3</sup> M. Bowry,<sup>5</sup> A. Bracco,<sup>6</sup> B. Bruyneel,<sup>7</sup> L. Corradi,<sup>4</sup> F. C. L. Crespi,<sup>6</sup> G. de Angelis,<sup>4</sup> P. Désesquelles,<sup>8</sup> J. Eberth,<sup>1</sup> E. Farnea,<sup>3</sup> E. Fioretto,<sup>4</sup> A. Gadea,<sup>9</sup> A. Gengelbach,<sup>10</sup> A. Giaz,<sup>6</sup> A. Görgen,<sup>11,12</sup> A. Gottardo,<sup>4</sup> J. Grebosz,<sup>13</sup> H. Hess,<sup>1</sup> P. R. John,<sup>2,3</sup> J. Jolie,<sup>1</sup> D. S. Judson,<sup>14</sup> A. Jungclaus,<sup>15</sup> W. Korten,<sup>12</sup> S. Lenzi,<sup>2</sup> S. Leoni,<sup>6</sup> S. Lunardi,<sup>2,3</sup> R. Menegazzo,<sup>3</sup> D. Mengoni,<sup>16,2,3</sup> C. Michelagnoli,<sup>2,3,†</sup> T. Mijatović,<sup>17</sup> G. Montagnoli,<sup>2,3</sup> D. Montanari,<sup>2,3,‡</sup> D. Napoli,<sup>4</sup> L. Pellegrì,<sup>6</sup> G. Pollarolo,<sup>18</sup> A. Pullia,<sup>6</sup> B. Quintana,<sup>19</sup> F. Radeck,<sup>1</sup> D. Rosso,<sup>4</sup> E. Şahin,<sup>4,§</sup> M. D. Salsac,<sup>12</sup> F. Scarlassara,<sup>2,3</sup> P.-A. Söderström,<sup>20,||</sup> A. M. Stefanini,<sup>4</sup> T. Steinbach,<sup>1</sup> O. Stezowski,<sup>21</sup> S. Szilner,<sup>17</sup> B. Szpak,<sup>13</sup> Ch. Theisen,<sup>12</sup> C. Ur,<sup>3</sup> V. Vandone,<sup>6</sup> and A. Wiens<sup>1</sup>

<sup>1</sup>*Institut für Kernphysik, Universität zu Köln, 50937 Köln, Germany*

<sup>2</sup>*Dipartimento di Fisica e Astronomia, Università di Padova, I-35131 Padova, Italy*

<sup>3</sup>*Istituto Nazionale di Fisica Nucleare, Sezione di Padova, I-35131 Padova, Italy*

<sup>4</sup>*Istituto Nazionale di Fisica Nucleare, Laboratori Nazionali di Legnaro, I-35020 Legnaro, Italy*

<sup>5</sup>*Department of Physics, University of Surrey, Guildford, Surrey GU2 7XH, United Kingdom*

<sup>6</sup>*Dipartimento di Fisica, Università di Milano and INFN Sezione di Milano, I-20133 Milano, Italy*

<sup>7</sup>*CEA Saclay, Service de Physique Nucleaire, F-91191 Gif-sur-Yvette, France*

<sup>8</sup>*Centre de Spectrométrie Nucléaire et de Spectrométrie de Masse (CSNSM), CNRS/IN2P3 and Université Paris-Sud, F-91405 Orsay Campus, France*

<sup>9</sup>*Instituto de Física Corpuscular, CSIC-Universidad de Valencia, E-46071 Valencia, Spain*

<sup>10</sup>*Department of Physics and Astronomy, Uppsala University, SE-75121 Uppsala, Sweden*

<sup>11</sup>*Department of Physics, University of Oslo, Post Office Box 1048 Blindern, N-0316 Oslo, Norway*

<sup>12</sup>*Institut de Recherche sur les lois Fondamentales de l'Univers (IRFU), CEA/DSM, Centre CEA de Saclay, F-91191 Gif-sur-Yvette Cedex, France*

<sup>13</sup>*Henryk Niewodniczański Institute of Nuclear Physics (PAN), PL-31342 Kraków, Poland*

<sup>14</sup>*Oliver Lodge Laboratory, University of Liverpool, Liverpool L69 7ZE, United Kingdom*

<sup>15</sup>*Instituto de Estructura de la Materia, CSIC, Madrid, E-28006 Madrid, Spain*

<sup>16</sup>*Nuclear Physics Research Group, University of the West of Scotland, High Street, Paisley PA1 2BE, Scotland, United Kingdom*

<sup>17</sup>*Ruđer Bošković Institute, HR-10 002 Zagreb, Croatia*

<sup>18</sup>*Dipartimento di Fisica Teorica dell'Università di Torino and INFN, I-10125 Torino, Italy*

<sup>19</sup>*Laboratorio de Radiaciones Ionizantes, Universidad de Salamanca, E-37008 Salamanca, Spain*

<sup>20</sup>*Department of Physics and Astronomy, Uppsala University, SE-75120 Uppsala, Sweden*

<sup>21</sup>*Université de Lyon, Université Lyon-1, CNRS/IN2P3, UMR5822, IPNL, F-69622 Villeurbanne Cedex, France*

(Received 14 September 2015; published 21 October 2015)

**Background:** Nuclear structure information for the neutron-rich actinide nuclei is important since it is the benchmark for theoretical models that provide predictions for the heaviest nuclei.

**Purpose:**  $\gamma$ -ray spectroscopy of neutron-rich heavy nuclei in the actinide region.

**Method:** Multinucleon-transfer reactions in  $^{70}\text{Zn} + ^{238}\text{U}$  and  $^{136}\text{Xe} + ^{238}\text{U}$  have been measured in two experiments performed at the INFN Legnaro, Italy. In the  $^{70}\text{Zn}$  experiment the high-resolution HPGe Clover Array (CLARA) coupled to the magnetic spectrometer PRISMA was employed. In the  $^{136}\text{Xe}$  experiment the high-resolution Advanced Gamma Tracking Array (AGATA) was used in combination with PRISMA and the Detector Array for Multinucleon Transfer Ejectiles (DANTE).

**Results:** The ground-state band (g.s. band) of  $^{240}\text{U}$  was measured up to the  $20^+$  level and a tentative assignment was made up to the  $(24^+)$  level. Results from  $\gamma\gamma$  coincidence and from particle coincidence analyses are shown. Moments of inertia (MoI) show a clear upbend. Evidence for an extended first negative-parity band of  $^{240}\text{U}$  is found.

**Conclusions:** A detailed comparison with latest calculations shows best agreement with cranked relativistic Hartree-Bogoliubov (CRHB) calculations for the g.s. band properties. The negative-parity band shows the characteristics of a  $K^\pi = 0^-$  band based on an octupole vibration.

DOI: [10.1103/PhysRevC.92.044319](https://doi.org/10.1103/PhysRevC.92.044319)

PACS number(s): 23.20.Lv, 25.70.Hi, 27.90.+b, 29.40.Gx

\*Corresponding author: [birkenbach@ikp.uni-koeln.de](mailto:birkenbach@ikp.uni-koeln.de)

<sup>†</sup>Present address: GANIL, CEA/DSM-CNRS/IN2P3, F-14076, Caen, France.

<sup>‡</sup>Present address: USIAS, Université de Strasbourg, IPHC-CNRS, F-67037 Strasbourg Cedex 2, France.

<sup>§</sup>Present address: Department of Physics, University of Oslo, P. O. Box 1048 Blindern, N-0316 Oslo, Norway.

<sup>||</sup>Present address: RIKEN Nishina Center, Wako, 351-0198 Saitama, Japan.

## I. INTRODUCTION

The heavy nuclei beyond the last doubly magic nucleus  $^{208}\text{Pb}$  in the actinide region from radium to nobelium show a variety of shapes in their ground states and at higher excitation energies. Besides a pronounced ground-state deformation in the quadrupole degree of freedom, also higher multipole orders are relevant and necessary to understand the basic properties of these nuclei. This is especially relevant for the extrapolation into the region of the heaviest elements, where a reduced deformation beyond the midshell region is a clear indicator for the next magic number. At this point not only the deformation as a function of proton number but also its dependence on the neutron number are of highest interest for the understanding of the shell closures of super-heavy elements.

Several theoretical predictions based on different models are put forward to describe shapes and collective excitations and await experimental verification. The ground-state energies, first excited states, and deformation parameters of a wide range of heavy nuclei from Ra up to the superheavy region were calculated in a macroscopic-microscopic approach [1]. The Yukawa-plus-exponential model is taken for the macroscopic part of the energy and the Strutinsky shell correction is used for the microscopic part. Detailed predictions for the even isotope chains  $^{226-236}\text{Th}$  and  $^{226-242}\text{U}$  are given with a minimum of excitation energy of the first  $2^+$  state and a maximum of deformation energy at  $N = 144, 146$  exactly at the border where experimental data are available.

A second macroscopic-microscopic model [2] is based on the Lublin-Strasbourg drop, the Strutinsky shell-correction method, and the Bardeen-Cooper-Schrieffer approach for pairing correlations used with the cranking model, taking into account a dynamical coupling of rotation with the pairing field. The results describe rotational bands in even-even Ra to Cn isotopes.

The g.s. band and low-lying alternative parity bands in the heaviest nuclei are also calculated within a cluster model [3]. The model is based on the assumption that reflection asymmetric shapes are produced by the motion of the nuclear system in the mass asymmetry coordinate. For the lightest  $N = 148$  isotones including  $^{240}\text{U}$ , detailed results on the levels of the ground-state rotational band and states of the alternative parity band are obtained. This includes transitional electric dipole, quadrupole, and octupole moments for the transitions from the ground state to the states of alternative parity band.

A very extensive theoretical study in the region from thorium to nobelium isotopes covered nearly all aspects of heavy actinide nuclei [4]. As part of the analysis, collective rotational excitations in the even-even nuclei  $^{226-236}\text{Th}$  and  $^{228-242}\text{U}$  were calculated employing the Gogny D1S force together with the constrained Hartree-Fock-Bogolyubov (HFB) mean-field method as well as the configuration mixing, blocking, and cranking HFB approaches. The experimental results from the present paper will be directly compared with the values for kinetic moments of inertia for the yrast normal deformed band of  $^{240}\text{U}$  as a function of rotational frequency calculated in this theoretical work.

Recent theoretical results on sequences of heavy nuclei from Th to No are obtained within self-consistent

relativistic Hartree-Bogolyubov mean-field calculations which provide a unified description of particle-hole and particle-particle correlations on a mean-field level [5]. Predictions are made for unknown ground-state axial quadrupole and hexadecapole moments along the isotopic chains of various actinide nuclei.

Octupole deformation properties of even-even  $^{220-240}\text{U}$  isotopes were also studied within the HFB mean-field framework employing realistic Gogny and Barcelona-Catania-Paris energy density functionals [6]. Here, an octupole collective Hamiltonian is used to obtain information on the evolution of excitation energies and  $E1$  and  $E3$  transition probabilities of the first negative-parity bandheads.

Afanasjev *et al.* [7,8] employed cranked relativistic Hartree-Bogolyubov (CRHB) calculations for a systematic study of pairing and normally deformed rotational bands of even-even and odd-mass actinides and transactinide nuclei within the relativistic (covariant) density functional theory (CDFT) framework. The calculations have been performed with the NL1 and NL3\* parametrizations of the relativistic mean-field Lagrangian. Pairing correlations are taken into account by the Brink-Booker part of the finite-range Gogny D1S force. The stabilization of octupole deformation at high spin is suggested by an analysis of discrepancies between theory and existing experimental information in the band-crossing region of  $A \approx 240$  nuclei.

The experimental results from in-beam  $\gamma$ -ray spectroscopy on excited states are either obtained in the vicinity of the few isotopes suited as target material in this mass region or have been measured after fusion evaporation reactions. In both cases mainly neutron-deficient actinide nuclei were investigated. Another approach is based on multinucleon-transfer (MNT) reactions as a tool for spectroscopy of heavy nuclei [9]. One type of experiments relies on the high resolving power and efficiency of a powerful  $\gamma$ -ray detector array to separate the  $\gamma$  rays from the multitude of reaction products and a tremendous background from fission [10]. A second group of measurements relies on few-nucleon transfer reactions with light oxygen beams and were successfully exploited to detect excited states, e.g., in neutron-rich  $^{236}\text{Th}$ ,  $^{240,242}\text{U}$  isotopes [11,12].  $\gamma$  rays were detected in coincidence with the outgoing transfer products. For the most neutron-rich cases the rotational g.s. band was detected up to spin 8 to  $10\hbar$ .

In this paper we report and discuss the results of two experiments based on different MNT reactions which were performed at the INFN Laboratori Nazionali di Legnaro (LNL) in order to study the structure of neutron-rich actinide nuclei. Experimental details and data analysis are described in the following two sections. Final results are deduced from  $\gamma$ -ray spectra in Sec. III. A detailed comparison with theoretical predictions and an interpretation of the new findings are given in Sec. IV before the paper closes with a summary and conclusions.

## II. EXPERIMENTAL SETUP

In the first experiment, the tandem van de Graaff accelerator in combination with the postaccelerator ALPI delivered a  $^{70}\text{Zn}$  beam with an energy of 460 MeV and a current of 2–2.5 pA.

TABLE I. Details of the experimental setups.

	Beam	
Particle	$^{70}\text{Zn}$	$^{136}\text{Xe}$
Energy	460 MeV	1000 MeV
Current	2–2.5 pA	2 pA
	Target	
Isotope	$^{238}\text{U}$	$^{238}\text{U}$
Backing		$^{93}\text{Nb}$
Target thickness	1 mg/cm <sup>2</sup>	1/2 mg/cm <sup>2</sup>
Backing thickness		0.8 mg/cm <sup>2</sup>

The beam impinged onto a 1-mg  $^{238}\text{U}$  target. The lighter beamlike reaction products were identified with the magnetic spectrometer PRISMA [13–15] and the  $\gamma$  rays were measured with the HPGe detector array CLARA [16]. The PRISMA spectrometer was placed at angles of  $61^\circ$  and  $64^\circ$  with respect to the beam axis that corresponds to the grazing angle for the multinucleon-transfer (MNT) reaction. The details of the targets and the beams are summarized in Table I. Details of the PRISMA analysis are reported in Ref. [17].

In the second experiment a beam of  $^{136}\text{Xe}$  with an energy of 1 GeV, accelerated by the PIAVE-ALPI accelerator complex, impinged on a  $^{238}\text{U}$  target. Again the PRISMA spectrometer was used to identify the beamlike particles following the MNT reaction. Experimental details are listed in Table I.  $\gamma$  Rays from excited states in both beam- and targetlike nuclei were measured, employing the high-resolution position-sensitive  $\gamma$ -ray spectrometer AGATA [18] in its demonstrator configuration [19] placed 23.5 cm from the target position. The array consisted of 15 large-volume electronically segmented high-purity Ge (HPGe) detectors in five triple cryostats [20]. The solid-angle coverage of the AGATA demonstrator was about 7% of  $4\pi$ . During the experiment, the count rate of each individual HPGe crystals was maintained between 20 and 30 kHz. A  $40 \times 60 \text{ mm}^2$  large DANTE (Detector Array for Multinucleon Transfer Ejectiles) microchannel plate detector [19] was mounted in the reaction plane covering the angle range which corresponds to the grazing angle for the targetlike reaction product in order to request a kinematic coincidence between the different reaction products.

### III. DATA ANALYSIS

Details of the PRISMA analysis are reported in Ref. [17] for the CLARA experiment and in Refs. [21,22] for the AGATA experiment. The measured quantities allow univocal identification and determination of the velocity vector for the individual lighter MNT reaction products. This enables the calculation of the element, the mass number, and the velocity vector of the binary reaction partner prior to neutron evaporation or fission has occurred. Therefore, by gating on a particular isotope of the lighter beamlike reaction products, the actinide targetlike reaction products are identified. In addition, the total kinetic energy loss (TKEL) in the system after the reaction was determined [14]. The resolution of the TKEL value is limited by the target thickness and the position uncertainty of the beam spot on the target. Most of

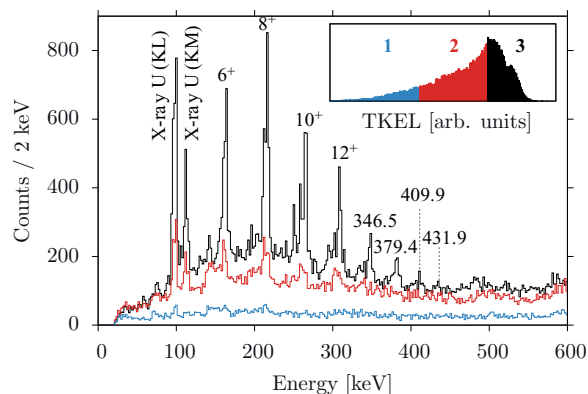


FIG. 1. (Color online) Single  $\gamma$ -ray spectra for  $^{68}\text{Zn}$  identified in PRISMA. The corresponding binary partner of the reaction is  $^{240}\text{U}$ . The spectra are Doppler corrected for the targetlike actinide nuclei. The inset shows the TKEL value in arbitrary units divided in three regions: 1, 2, and 3. The color code of the  $\gamma$ -ray spectra corresponds to the three different TKEL regions.

the produced actinide nuclei are excited up to an energy higher than the neutron-separation energy which enables neutron evaporation. Nonetheless, a gate on the TKEL value is helpful to constrain the excitation energy of the nuclei and to suppress fission events [21].

Results from the  $^{70}\text{Zn}$  experiment are shown in Fig. 1. The selected nucleus after the identification with PRISMA is  $^{68}\text{Zn}$  and the corresponding binary partner is  $^{240}\text{U}$ . The  $\gamma$ -ray spectra are Doppler corrected for the targetlike actinide nuclei. The TKEL distribution is given in the inset. It is divided into three regions. The  $\gamma$ -ray spectrum corresponding to TKEL region 1 (blue [gray, bottom]) shows a constant structureless background caused by fission [21]. The  $\gamma$ -ray spectrum of region 2 (red [gray, middle]) shows high background contributions and indications of overlapping peaks. Events from fission and neutron evaporation are visible. In the  $\gamma$ -ray spectrum corresponding to the third TKEL cut (black [top]), distinct peaks of  $^{238-240}\text{U}$  can be identified. Known transitions from  $^{240}\text{U}$  dominate and are indicated in the figure. Decays of the g.s. band up to the  $12^+$  state are visible, and the energies compare well with previous measurements [11]. In addition, unobserved lines of the rotational sequence can be identified.

To ensure that different  $\gamma$ -ray decays are part of the g.s. band, particle gated  $\gamma\gamma$  coincidences are analyzed. The overall projection of the  $\gamma\gamma$  matrix is shown in the top part of Fig. 2. Similar to the single spectrum (see Fig. 1) the  $\gamma$  rays from the transitions of the g.s. band in  $^{240}\text{U}$  are clearly visible. In addition, candidates for the decay of the  $14^+$  up to the  $20^+$  levels are visible. By gating on the different energies up to 381 keV the expected coincidences show up; see Figs. 2(b)–2(g). In Fig. 2(h) the sum of all coincidence gates is shown. Up to an energy of 409.9 keV, intraband transitions are identified.

The second experiment employed the heavier  $^{136}\text{Xe}$  beam with an energy of 1 GeV. The AGATA demonstrator was used for  $\gamma$ -ray detection and in addition to PRISMA the DANTE detector was mounted inside the scattering chamber. The trigger requested a signal from the focal plane detector of PRISMA. Data from all validated events including the

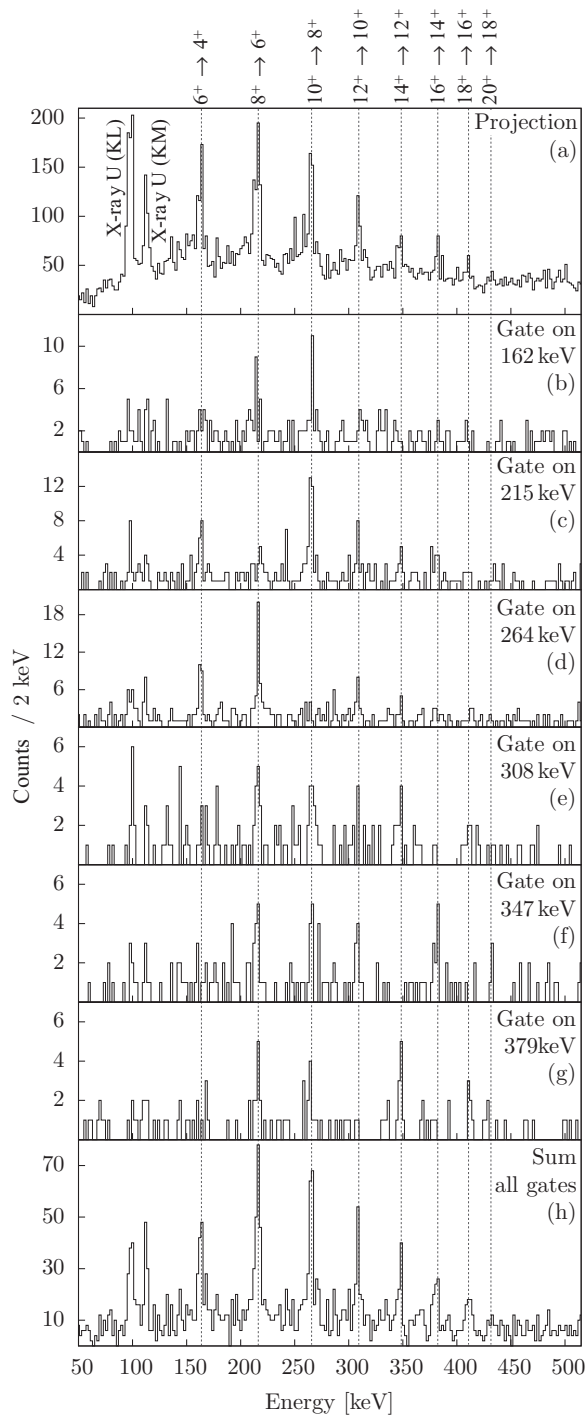


FIG. 2. Particle gated coincidence spectra for  $^{240}\text{U}$  from the CLARA experiment. Projection on one axis of the  $\gamma\gamma$  matrix (a), gate on 162 keV (b), gate on 215 keV (c), gate on 264 keV (d), gate on 307 keV (e), gate on 347 keV (f), gate on 381 keV (g), and the sum of all the shown gated spectra (h).

full information of the digitized preamplifier responses of all AGATA channels were acquired and stored. This opened the opportunity to optimize energy and timing settings by replaying the complete experiment. An improved Doppler correction, possible due to the position resolution and tracking

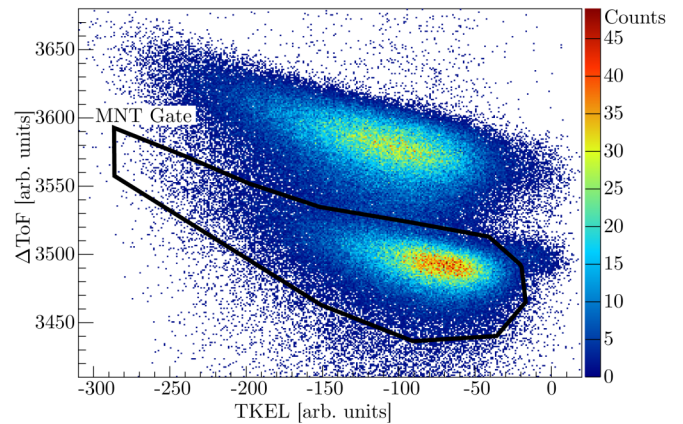


FIG. 3. (Color online) Two-dimensional (2D) histogram of  $\Delta\text{ToF}$  and TKEL values for all events with  $^{134}\text{Xe}$  identified in PRISMA. The 2D gate selecting primarily MNT events is plotted as a solid black line.

capabilities of the AGATA spectrometer [23], was performed. By gating on the prompt time peak between AGATA and PRISMA, random background could be significantly suppressed. Similar to the Zn experiment, the targetlike actinide nuclei are selected by gating on the binary partner identified in PRISMA. As introduced in Ref. [21], the time-of-flight difference ( $\Delta\text{ToF}$ ) between the two reaction products was measured at the entrance detector of PRISMA and the DANTE detector inside the scattering chamber. A 2D histogram in which  $\Delta\text{ToF}$  and the calculated TKEL are correlated is shown in Fig. 3 for  $^{134}\text{Xe}$ . A gate is applied to select transfer events.

The resulting  $\gamma$ -ray spectra are presented in Ref. [21] (see Fig. 6 for  $^{238}\text{U}$  and Fig. 13 for  $^{240}\text{U}$  in Ref. [21]) in order to demonstrate the selectivity and quality of the MNT reaction; however, no results of the following detailed analysis were given. Different isotopes, namely  $^{238-240}\text{U}$ , contribute to the  $\gamma$ -ray spectrum of  $^{240}\text{U}$ . An additional gate on the TKEL allows suppression of neutron evaporation.

The resulting spectra are shown in Fig. 4 for  $^{238}\text{U}$  and in Fig. 5 for  $^{240}\text{U}$ . The spectrum of  $^{238}\text{U}$  shows  $\gamma$  rays from the de-excitation of states belonging to the g.s. band up to spin  $22^+$ . In addition, transitions from the first negative-parity band are observed up to spin  $17^-$ , and the ( $I \rightarrow I - 1$ ) interband transitions are clearly visible.

In the  $\gamma$ -ray spectrum of  $^{240}\text{U}$  the same transitions as in the  $\gamma\gamma$  sum spectrum of Fig. 2 are seen up to the one with 431.9 keV. Additional weaker lines are visible in the spectrum which will be tentatively assigned to decays from higher spin states. Several peaks are candidates for the decay of states from the first negative-parity band, similar to the energies reported in Ref. [11]. Unfortunately, some of the observed lines are close in energy with decays of the first  $2^+$  and  $4^+$  states of the binary partner  $^{134}\text{Xe}$ . Energies are shifted and their line width is broadened due to the Doppler correction made for  $^{240}\text{U}$ . Two interband transitions from the  $3^-$  state, the  $I \rightarrow I \pm 1$  decays, are visible. For the decays from the  $5^-$ ,  $7^-$ , and  $9^-$  states only the  $I \rightarrow I - 1$  transition could be identified. For none of the lines is the statistics sufficient to perform a  $\gamma\gamma$  analysis and the proposed assignment is therefore tentative.

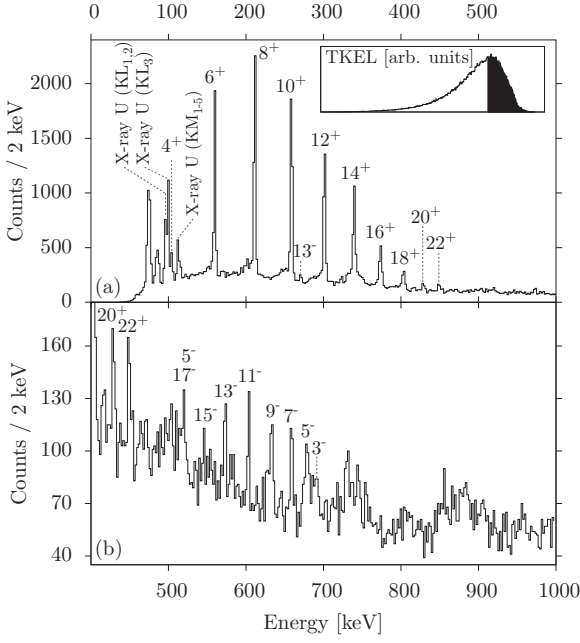


FIG. 4. Doppler-corrected single  $\gamma$ -ray spectrum for  $^{238}\text{U}$  gated by  $^{136}\text{Xe}$  identified in PRISMA. Beside the applied gate for MNT an additional cut on the TKEL value was performed (see black region in inset).

In summary, the spin assignment for the observed transitions of the ground-state rotational band up to spin  $20^+$  are based on the  $\gamma\gamma$  coincidences relation (see Fig. 2). All transitions were clearly observed in the CLARA and AGATA

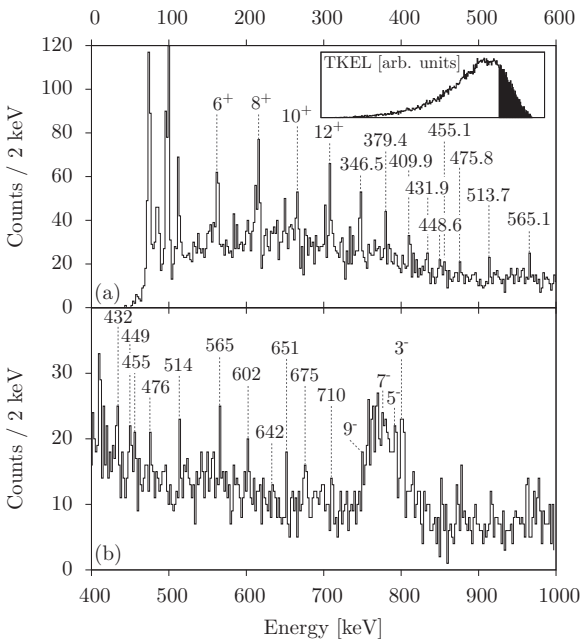


FIG. 5. Doppler-corrected single  $\gamma$ -ray spectrum for  $^{240}\text{U}$  gated by  $^{134}\text{Xe}$  identified in PRISMA. Beside the applied gate for MNT (see Fig. 3) an additional cut on the TKEL value was performed (see black region in inset).

TABLE II.  $\gamma$ -ray energies and spin assignments for  $^{240}\text{U}$ . Relative intensities are determined from the  $\gamma\gamma$  projection; see Fig. 2(a).

This work			Ishii <i>et al.</i> [11]	
$E_\gamma$ [keV]	Rel. intensity	$I_i \rightarrow I_f$	$E_\gamma$ [keV]	$I_i \rightarrow I_f$
161.9 (10)	0.630 (86)	$6^+ \rightarrow 4^+$	105.6 (1)	$4^+ \rightarrow 2^+$
215.4 (10)	1.00 (11)	$8^+ \rightarrow 6^+$	162.1 (1)	$6^+ \rightarrow 4^+$
263.9 (10)	0.84 (10)	$10^+ \rightarrow 8^+$	215.4 (1)	$8^+ \rightarrow 6^+$
307.5 (10)	0.495 (70)	$12^+ \rightarrow 10^+$	264.1 (2)	$10^+ \rightarrow 8^+$
346.5 (10)	0.289 (54)	$14^+ \rightarrow 12^+$	307.6 (3)	$12^+ \rightarrow 10^+$
379.4 (10)	0.228 (49)	$16^+ \rightarrow 14^+$		
409.9 (10)	0.138 (44)	$18^+ \rightarrow 16^+$		
431.9 (10)	0.068 (40)	$20^+ \rightarrow 18^+$		
448.6 (10)		$(22^+ \rightarrow 20^+)$		
(455.1) (10)		$(24^+ \rightarrow 22^+)$		
475.8 (10)				
513.7 (10)		$(21^- \rightarrow 20^+)$		
565.1 (10)		$(19^- \rightarrow 18^+)$		
601.6 (10)		$(17^- \rightarrow 16^+)$		
(642.0) (10)		$(15^- \rightarrow 14^+)$		
675.2 (10)		$(13^- \rightarrow 12^+)$		
697.2 (19)		$3^- \rightarrow 4^+$	696.4 (5)	$3^- \rightarrow 4^+$
710.0 (10)		$(11^- \rightarrow 10^+)$		
749.0 (20)		$9^- \rightarrow 8^+$	747.5 (3)	$9^- \rightarrow 8^+$
778.1 (32)		$7^- \rightarrow 6^+$	774.5 (3)	$7^- \rightarrow 6^+$
791.9 (35)		$5^- \rightarrow 4^+$	794.0 (3)	$5^- \rightarrow 4^+$
800.8 (20)		$3^- \rightarrow 2^+$	801.9 (5)	$3^- \rightarrow 2^+$

experiments. The two transitions at 449 and 455 keV most probably originate from the decay of the  $22^+$  and  $24^+$  states of the g.s. band. Level energies for the  $3^-$ ,  $5^-$ ,  $7^-$ , and  $9^-$  states are taken from Ref. [11] due to experimental difficulties explained above. All the measured  $\gamma$ -ray energies and the assignments are listed in Table II; included are also results reported in Ref. [11]. The corresponding level scheme is presented in Fig. 6.

#### IV. INTERPRETATION

In Fig. 7, a comparison between the energies of the g.s. band levels obtained in this experiment, the data obtained by Ishii *et al.* [11] and theoretical predictions are shown. The experimental data agree well with the level scheme calculated within the cluster model [3]. For the macroscopic-microscopic model two results are given [2]. The dynamical coupling of rotation and pairing mode agrees well with the experimental data. The level energies predicted by the  $I(I+1)$  rule are increasingly too high as a function of spin underlining the necessary coupling as reported in Ref. [2].

A refined comparison between the experimental results and predictions from theory is based on the kinetic moment of inertia  $J_{\text{kin}}$  (MoI), which is deduced from the transition energies  $E_\gamma$  of the ground-state rotational band [24–26]:

$$J_{\text{kin}} = \frac{I}{\omega} = \frac{\hbar^2 (2I-1)}{E_\gamma (I \rightarrow I-2)}. \quad (1)$$

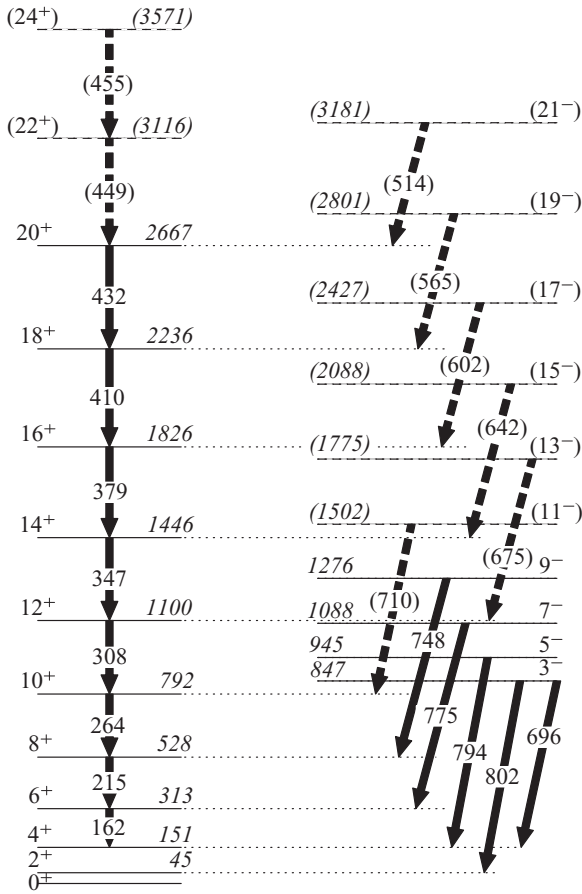


FIG. 6. Proposed extended level scheme for  $^{240}\text{U}$ . Spin and parity assignments are taken from Ref. [11] or based on  $\gamma\gamma$ -coincidence relationships. Tentative assignments are given in brackets.

The rotational frequencies are calculated using the expression

$$\hbar\omega_{\text{kin}} = \frac{E_\gamma}{\sqrt{I(I+1)} - \sqrt{(I-2)(I-1)}}. \quad (2)$$

The deviations in energy differences between the consecutive rotational transition energies are used as the basis to define a dynamic MoI  $J_{\text{dyn}}$ :

$$J_{\text{dyn}} = \frac{dI}{d\omega} \approx \frac{\hbar^2 \Delta I}{\Delta E_\gamma} = \frac{4\hbar^2}{E_{\gamma 1} - E_{\gamma 2}} \quad (3)$$

with  $E_{\gamma 1} = E(I \rightarrow I-2)$  and  $E_{\gamma 2} = E(I-2 \rightarrow I-4)$ . The corresponding dynamic rotational frequencies are defined as

$$\hbar\omega_{\text{dyn}} = \frac{E_{\gamma 1} + E_{\gamma 2}}{4}. \quad (4)$$

With the following parametrization by Harris [27], the kinetic and dynamic MoI are found:

$$\begin{aligned} J_{\text{kin}} &= \mathcal{J}_1 + \mathcal{J}_2 \omega^2, \\ J_{\text{dyn}} &= \mathcal{J}_1 + 3 \mathcal{J}_2 \omega^2. \end{aligned} \quad (5)$$

The transitions below the  $4^+$  state are not visible in the  $\gamma$ -ray spectra due to decay by internal electron conversion. For the two lowest unobserved transitions, the energies and

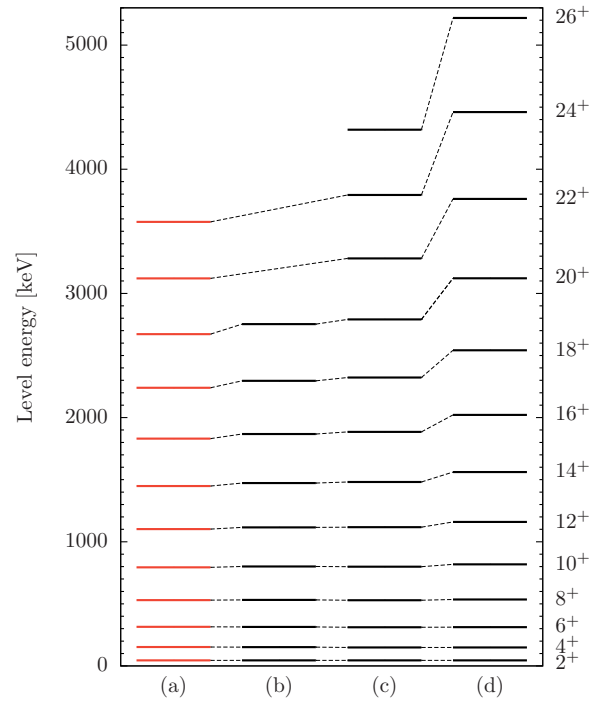


FIG. 7. (Color online) Comparison of experimentally determined level energies with theoretical predictions. (a) Data from this work. (b) Theoretical prediction from cluster model [3], and from a macroscopic-microscopic approach [2] with (c) dynamical coupling or (d)  $I(I+1)$  sum rule.

spin-parity assignments from Ishii *et al.* [11] [ $E_\gamma(4^+ \rightarrow 2^+) = 105.6$  keV] and previous  $\alpha$ -decay [28] and  $^{238}\text{U}(t, p)$  [29] measurements [ $E_\gamma(2^+ \rightarrow 0^+) = 45(1)$  keV] are taken.

The spins for the ground-state rotational band are linked to the rotational frequency and the Harris fit parameters [30]:

$$I = \mathcal{J}_1 \omega + \mathcal{J}_2 \omega^3 + \frac{1}{2}. \quad (6)$$

In this way the transition energies of the  $2^+ \rightarrow 0^+$  and  $4^+ \rightarrow 2^+$  states are determined to be 45.5(3) and 104.9(6) keV, respectively. These values agree well with the given literature values.

The Harris parametrization provides a good indicator for a comparison of the experimental MoI with the regular  $I(I+1)$  behavior. Both MoI values,  $J_{\text{kin}}$  and  $J_{\text{dyn}}$  [see Eq. (5)], are fitted to the experimental data up to the  $12^+$  g.s. band state. The determined parameters are  $\mathcal{J}_1 = (65.8 \pm 0.4) \hbar^2 \text{MeV}^{-1}$  and  $\mathcal{J}_2 = (369 \pm 27) \hbar^4 \text{MeV}^{-3}$  for  $^{240}\text{U}$ . The ground-state value of the MoI compares well with the value of  $66.9 \hbar^2 \text{MeV}^{-1}$  calculated by Sobczewski *et al.* [1].

The fits and the experimental data points are shown in Fig. 8. The evolution of the moments of inertia as a function of rotational frequency  $\omega$  are also shown for the lighter even-even isotopes  $^{236,238}\text{U}$  (experimental values for  $^{236,238}\text{U}$  are taken from Ref. [31]). The  $\mathcal{J}_1$  values are similar for all three isotopes; only the  $\mathcal{J}_2$  value of  $^{240}\text{U}$  is smaller than for  $^{236,238}\text{U}$ . For the higher transitions beyond the  $12^+$  state an increasing deviation to the fit, an upbend, is observed. The smooth upbend [32] in  $^{240}\text{U}$  beyond the  $18^+$  g.s. band state is more pronounced

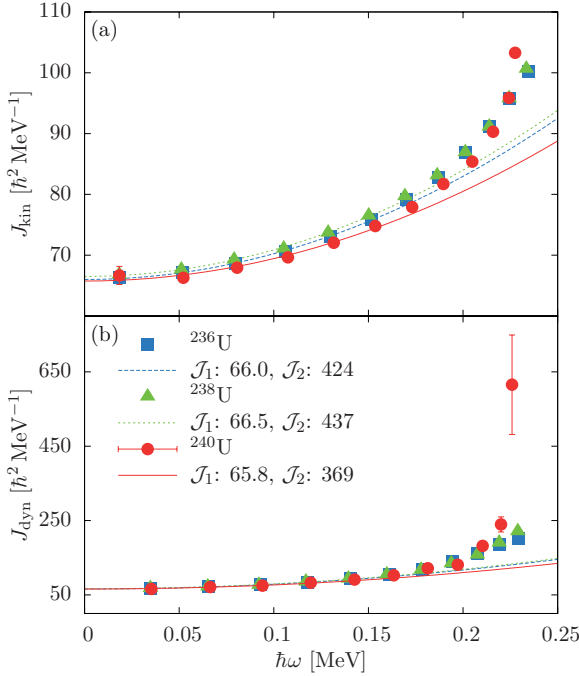


FIG. 8. (Color online) Fits employing the Harris parametrization of  $J_{\text{kin}}$  and  $J_{\text{dyn}}$  for the U isotopic chain from  $^{236}\text{U}$  to  $^{240}\text{U}$ . Data for  $A = 236$  and  $238$  are taken from Ref. [31].

than in the corresponding neutron-deficient isotopes along the U isotopic chain. A similar behavior was also observed in neutron-rich Pu, Cm, and Cf isotopes [8,33].

The experimental kinetic MoI of  $^{240}\text{U}$  is compared to kinetic MoIs from various theoretical calculations (red [gray] data points versus black lines in Fig. 9). For the model by Delaroche *et al.* [4] the absolute numbers of the kinetic MoI are consistently higher than the experimentally determined MoI. The slope of the upbend of the kinetic MoI around a rotational frequency of  $0.2 \text{ MeV } \hbar^{-1}$  is in reasonable agreement with the experimental data. The macroscopic-microscopic model by Nerlo-Pomorska *et al.* [2] underestimates the beginning of the experimental upbend. The cluster model by Shneidman *et al.* [3] does not include predictions for the behavior at higher rotational frequencies. The behavior of the MoI is best reproduced by the relativistic CRHB approach by Afanasjev *et al.* [7,8]. Up to  $18 \hbar$  the LN(NL3\*) parametrization is in very good agreement with the data points, while at even higher spins the LN(NL1) parametrization provides the best agreement.

Both CRHB + LN(NL1) and CRHB + LN(NL3\*) calculations suggest a sharp increase of the kinetic MoI above  $\hbar\omega \approx 0.2 \text{ MeV}$ . Indeed a change of slope is observed at this energy. This upbend is predominantly due to the alignment of  $i_{13/2}$  protons and  $j_{15/2}$  neutrons which take place at similar rotational frequencies [7].

Besides the extension of the g.s. band, the AGATA experiment also yielded results on the first negative-parity (octupole) band. The first states of the alternative-parity band of  $^{240}\text{U}$  were reported in Ref. [11] at higher energies than in  $^{236,238}\text{U}$ .

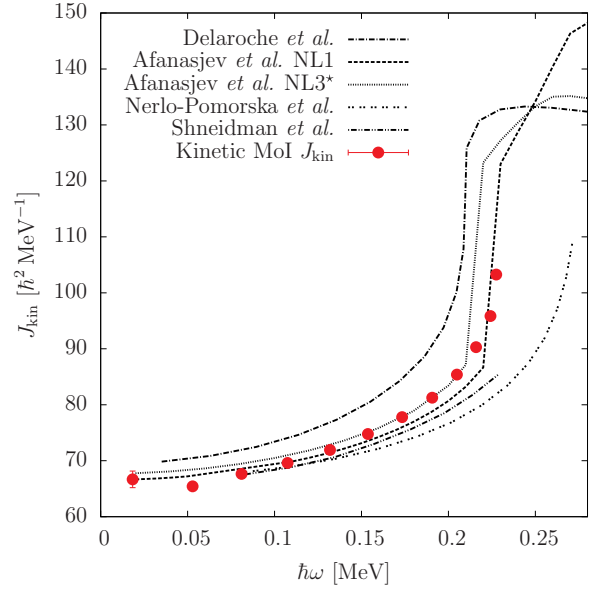


FIG. 9. (Color online) Kinetic MoI,  $J_{\text{kin}}$ , from this work (red [gray] points) in comparison to various theoretical predictions. The CRHB + LN(NL1) and CRHB + LN(NL3\*) calculations by Afanasjev *et al.* best reproduce the experimental data. The experimental values for the decays of the  $4^+$  and  $2^+$  g.s. band states were taken from the literature [11,28,29].

To disentangle the octupole correlations or deformation from octupole vibration, properties of the negative-parity band were scrutinized. In the case of strong octupole correlations an alternating parity band occurs. Here, the odd-spin negative-parity states lie much lower in excitation energy and form an alternating parity band together with the adjacent positive-parity even-spin states. A characteristic feature of vibrational octupole motion is that the negative-parity states appear at higher excitation energies and are well separated from the positive-parity states [34]. In the top panel of Fig. 10, the energy staggering (or parity splitting)  $S(I)$  between the odd-spin, negative-parity and even-spin, positive-parity bands of  $^{236,238,240}\text{U}$  is presented.

$$S(I) = E(I) - \frac{E(I-1)(I+1) + E(I+1)I}{2I+1}. \quad (7)$$

$S(I)$  displays to which extent the odd spin  $I$  of the negative-parity band has an excitation energy located in between those of the two neighboring even-spin states with spins  $I-1$  and  $I+1$ , therefore parameterizing to which extend the two bands of opposite parity can be regarded as a single, rotational octupole excitation [33,35]. The staggering observed in the three uranium isotopes is largest for  $^{240}\text{U}$  at low spins as expected for a vibrational band. With increasing spin the  $S(I)$  value comes down to values between  $^{236}\text{U}$  and  $^{238}\text{U}$ . A similar behavior is found at the even-even  $^{242,244}\text{Pu}$  isotopes [33].

Another indicator is given by the ratio between the rotational frequencies of the positive- and the negative-parity bands:

$$\frac{\omega^-(I)}{\omega^+(I)} = 2 \frac{E^-(I+1) - E^-(I-1)}{E^+(I+2) - E^+(I-2)}. \quad (8)$$

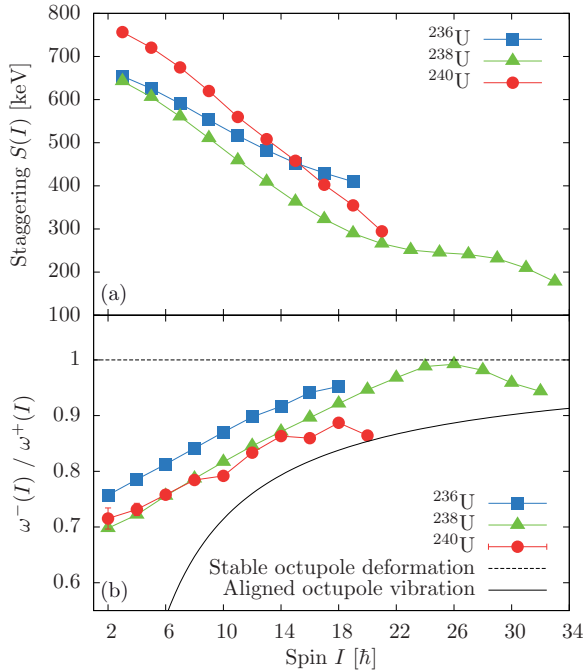


FIG. 10. (Color online) (a) Staggering  $S(I)$  in the three uranium isotopes  $^{236}\text{U}$ ,  $^{238}\text{U}$ , and  $^{240}\text{U}$ . The staggering parameter for  $^{240}\text{U}$  continues to decrease up to the highest spins while  $S(I)$  saturates in the lighter U isotopes. (b) Ratio of rotational frequencies of the positive- and negative-parity bands as a function of spin.  $^{236,238}\text{U}$  data taken from Ref. [31].

Values are presented in the bottom panel of Fig. 10. The ratio approaches 1 for a stable octupole deformation and is  $(2I - 5)/(2I + 1)$  in the limit of an aligned octupole vibration [35].

Another approach to evaluate the behavior of the negative-parity band was introduced by Jolos and von Brentano [34]. The model suggests a formula for the angular momentum dependence of the parity splitting in alternating parity bands from a solution of the one-dimensional Schrödinger equation with a double-minimum potential. The normalized parity splitting is defined as  $\Delta\epsilon(I) \equiv \Delta E(I)/\Delta E(2)$  with  $\Delta E(I)$  being the parity splitting averaged over three neighboring values of  $I$ :

$$\Delta\epsilon(I) = \exp \left[ -\frac{I(I+1)}{\mathcal{J}_0(\mathcal{J}_0+1)[1+aI(I+1)]} + \frac{6}{\mathcal{J}_0(\mathcal{J}_0+1)(1+6a)} \right]. \quad (9)$$

The deduced values of  $-\ln[\Delta\epsilon(I)]$  for  $^{236-240}\text{U}$  with two fits for  $a = 0$  (dashed lines) and  $a$  as a free parameter (solid line) are plotted in Fig. 11. The general behavior for all three isotopes is comparable: Starting with a linear increase at low spins, for higher spin values a positive parameter  $a$  describes the data. This behavior is unambiguously assigned to octupole vibrational nuclei in Ref. [34]. Moreover, the good agreement of the fit and the data supports the validity of the experimental findings.

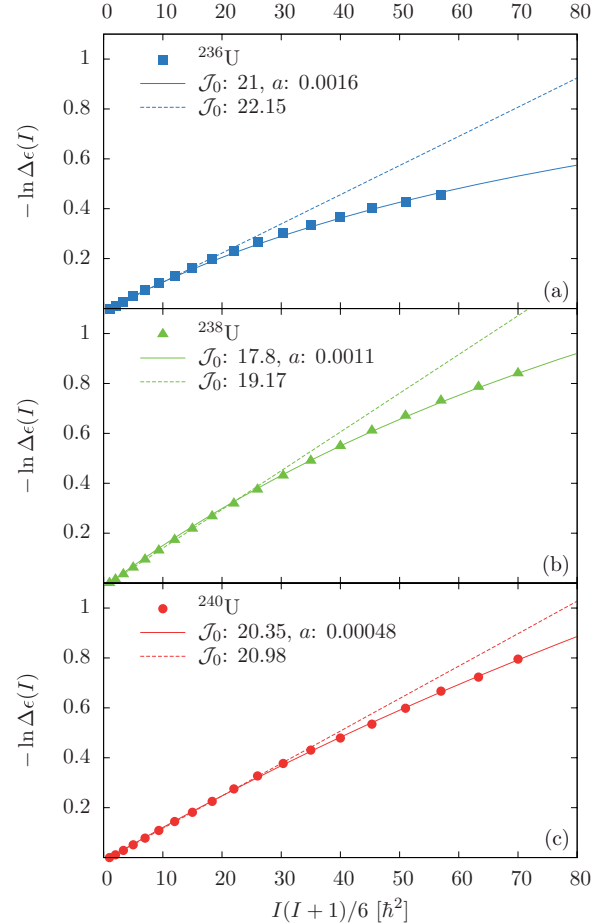


FIG. 11. (Color online) Experimental data, parametrized as  $-\ln \Delta\epsilon(I)$  vs  $I(I+1)/6$  for  $^{236}\text{U}$  (a),  $^{238}\text{U}$  (b), and  $^{240}\text{U}$  (c). Fits with  $a = 0$  are shown as dashed lines; solid curves include  $a$  as a free parameter.  $^{236,238}\text{U}$  data taken from Ref. [31].

## V. SUMMARY AND CONCLUSIONS

In summary, we have measured  $\gamma$  rays in  $^{240}\text{U}$  following multinucleon transfer induced by  $^{70}\text{Zn} + ^{238}\text{U}$  and  $^{136}\text{Xe} + ^{238}\text{U}$  reactions. The magnetic spectrometer PRISMA was employed, in the first experiment coupled to the  $\gamma$ -ray detector CLARA and in the second one coupled to the  $\gamma$ -ray tracking detector AGATA together with the particle detector DANTE. Neutron-rich  $^{240}\text{U}$  was selected by gating on the binary partner  $^{134}\text{Xe}$  identified by PRISMA. Neutron-evaporation channels were suppressed by restrictions on the TKEL value. Conditions on particle-particle coincidences were employed to suppress the fission-induced background. The information on the beamlike reaction products from PRISMA was combined with a Doppler correction for the targetlike nuclei to study the structure of  $^{240}\text{U}$ . Especially for the second experiment, the advanced opportunities of the novel  $\gamma$ -ray tracking technique yielded improved Doppler-corrected  $\gamma$ -ray spectra.

The heavy-ion-induced reactions involved higher angular momentum, allowing an extension of the g.s. band of  $^{240}\text{U}$  up to the  $20^+$  state, and tentative assignments up to the  $(24^+)$  state were made. The kinetic and dynamic moments of inertia were



extracted and compared to theoretical predictions. The low-energy, low-spin part is well described by both cluster models and macroscopic-microscopic approaches. The population of high-spin states allowed for the first time the observation of an upbend at rotational frequencies around  $0.2 \text{ MeV } \hbar^{-1}$ . This behavior is best reproduced by recent relativistic mean-field calculations within the CDFT framework [7,8].

Despite experimental difficulties, there is convincing evidence for the  $K^\pi = 0^-$  negative-parity band which was extended up to a tentatively assigned  $(21^-)$  state. Three different parametrizations such as energy staggering and parity splitting between the g.s. band and the negative-parity band yield consistent results. The experimental findings suggest that the newly observed band is interpreted best as a collective octupole vibrational excitation. This interpretation is supported by the similarities with the neighboring  $^{236-240}\text{U}$  isotopes.

Our new experimental results are a further step in the understanding of more neutron-rich uranium isotopes and actinide nuclei in general. However, further experimental evidence is highly desirable and improved experiments with

higher statistics are needed to corroborate the results. For this endeavour high-efficiency detection devices are mandatory to overcome the reported low cross sections in the microbarn region for these type of reactions [21].

#### ACKNOWLEDGMENTS

The research leading to these results has received funding from the German Bundesministerium für Bildung und Forschung (BMBF) under Contract No. 05P12PKFNE TP4, the European Union Seventh Framework Programme (FP7/2007-2013) under Grant No. 262010-ENSAR, and the Spanish Ministerio de Ciencia e Innovación under Contract No. FPA2011-29854-C04. A.V. thanks the Bonn-Cologne Graduate School of Physics and Astronomy (BCGS) for financial support. One of the authors (A. Gadea) was supported by MINECO, Spain, under Grants No. FPA2011-29854-C04 759 and No. FPA2014-57196-C5; Generalitat Valenciana, Spain, under Grant No. PROMETEOII/2014/019; and EU under the FEDER program.

- 
- [1] A. Sobczewski, I. Muntian, and Z. Patyk, *Phys. Rev. C* **63**, 034306 (2001).
- [2] B. Nerlo-Pomorska, K. Pomorski, and J. Bartel, *Phys. Rev. C* **84**, 044310 (2011).
- [3] T. M. Shneidman, G. G. Adamian, N. V. Antonenko, and R. V. Jolos, *Phys. Rev. C* **74**, 034316 (2006).
- [4] J.-P. Delaroche, M. Girod, H. Goutte, and J. Libert, *Nucl. Phys. A* **771**, 103 (2006).
- [5] D. Vretenar, T. Niksic, and P. Ring, *Int. J. Mod. Phys. E* **19**, 548 (2010).
- [6] L. M. Robledo and R. R. Rodríguez-Guzmán, *J. Phys. G: Nucl. Part. Phys.* **39**, 105103 (2012).
- [7] A. V. Afanasjev and O. Abdurazakov, *Phys. Rev. C* **88**, 014320 (2013).
- [8] A. V. Afanasjev, *Phys. Scr.* **89**, 054001 (2014).
- [9] L. Corradi, G. Pollaro, and S. Szilner, *J. Phys. G: Nucl. Part. Phys.* **36**, 113101 (2009).
- [10] J. F. C. Cocks *et al.*, *J. Phys. G: Nucl. Part. Phys.* **26**, 23 (2000).
- [11] T. Ishii, S. Shigematsu, M. Asai, A. Makishima, M. Matsuda, J. Kaneko, I. Hossain, S. Ichikawa, T. Kohno, and M. Ogawa, *Phys. Rev. C* **72**, 021301 (2005).
- [12] T. Ishii *et al.*, *Phys. Rev. C* **76**, 011303 (2007).
- [13] A. Stefanini *et al.*, *Nucl. Phys. A* **701**, 217 (2002).
- [14] S. Szilner *et al.*, *Phys. Rev. C* **76**, 024604 (2007).
- [15] L. Corradi *et al.*, *Nucl. Instrum. Methods Phys. Res., Sect. B* **317**, 743 (2013).
- [16] A. Gadea *et al.*, *J. Phys. G: Nucl. Part. Phys.* **31**, S1443 (2005).
- [17] K. Geibel, Ph.D. thesis, Universität zu Köln, 2012.
- [18] S. Akkoyun *et al.*, *Nucl. Instrum. Methods Phys. Res., Sect. A* **668**, 26 (2012).
- [19] A. Gadea *et al.*, *Nucl. Instrum. Methods Phys. Res., Sect. A* **654**, 88 (2011).
- [20] A. Wiens, H. Hess, B. Birkenbach, B. Bruyneel, J. Eberth, D. Lersch, G. Pascovici, P. Reiter, and H.-G. Thomas, *Nucl. Instrum. Methods Phys. Res., Sect. A* **618**, 223 (2010).
- [21] A. Vogt *et al.*, *Phys. Rev. C* **92**, 024619 (2015).
- [22] B. Birkenbach, Ph.D. thesis, Universität zu Köln, 2014.
- [23] A. Lopez-Martens, K. Hauschild, A. Korichi, J. Roccas, and J.-P. Thibaud, *Nucl. Instrum. Methods Phys. Res., Sect. A* **533**, 454 (2004).
- [24] J. E. Draper, F. S. Stephens, M. A. Deleplanque, W. Korten, R. M. Diamond, W. H. Kelly, F. Azaiez, A. O. Macchiavelli, C. W. Beausang, E. C. Rubel, J. A. Becker, N. Roy, E. A. Henry, M. J. Brinkman, A. Kuhnert, and S. W. Yates, *Phys. Rev. C* **42**, R1791 (1990).
- [25] J. A. Becker, E. A. Henry, A. Kuhnert, T. F. Wang, S. W. Yates, R. M. Diamond, F. S. Stephens, J. E. Draper, W. Korten, M. A. Deleplanque, A. O. Macchiavelli, F. Azaiez, W. H. Kelly, J. A. Cizewski, and M. J. Brinkman, *Phys. Rev. C* **46**, 889 (1992).
- [26] G. Hackman, T. L. Khoo, M. P. Carpenter, T. Lauritsen, A. Lopez-Martens, I. J. Calderin, R. V. F. Janssens, D. Ackermann, I. Ahmad, S. Agarwala, D. J. Blumenthal, S. M. Fischer, D. Nisius, P. Reiter, J. Young, H. Amro, E. F. Moore, F. Hannachi, A. Korichi, I. Y. Lee, A. O. Macchiavelli, T. Døssing, and T. Nakatsukasa, *Phys. Rev. Lett.* **79**, 4100 (1997).
- [27] S. M. Harris, *Phys. Rev.* **138**, B509 (1965).
- [28] B. Back, E. Flynn, O. Hansen, R. Casten, and J. Garrett, *Nucl. Phys. A* **217**, 116 (1973).
- [29] C. E. Bemis Jr., J. Halperin, and R. Eby, *J. Inorg. Nucl. Chem.* **31**, 599 (1969).
- [30] P. Reiter *et al.*, *Phys. Rev. Lett.* **82**, 509 (1999).
- [31] Evaluated Nuclear Structure Data File (ENSDF) [<http://www.nndc.bnl.gov/ensdf/>].
- [32] W. Spreng, F. Azgui, H. Emling, E. Grosse, R. Kulessa, C. Michel, D. Schwalm, R. S. Simon, H. J. Wollersheim, M. Mutterer, J. P. Theobald, M. S. Moore, N. Trautmann, J. L. Egido, and P. Ring, *Phys. Rev. Lett.* **51**, 1522 (1983).
- [33] I. Wiedenhöver *et al.*, *Phys. Rev. Lett.* **83**, 2143 (1999).
- [34] R. V. Jolos and P. von Brentano, *Phys. Rev. C* **49**, R2301 (1994).
- [35] W. Nazarewicz and P. Olanders, *Nucl. Phys. A* **441**, 420 (1985).